RSC Advances

PAPER

View Article Online
View Journal | View Issue

Cite this: *RSC Adv.*, 2026, **16**, 24747

Closing and coupling: metal linked biliazine dimers

Towhidi Illius Jeaydi,[a] Wei-Yuan Chen,[b] Michael D. Tedesco,[a] Briana R. Schrage,[a] Victor N. Nemykin[b] and Christopher J. Ziegler *[a]

Received 25th February 2026
Accepted 1st May 2026

DOI: 10.1039/d6ra01668e

rsc.li/rsc-advances

Biliazines, tetradentate chelates similar to the bilin class of heme metabolites, are ring open phthalocyanine analogs where the chelate ring is closed by a hydrogen bond. Linked dimers of biliazines, incorporating both pyrazole and indazole units, can be produced *via* a self-assembly reaction between the diiminoisoindoline-pyrazole and indazole chelate precursors and zinc ion in a 4 : 3 ratio. The dimers are comprised of zinc metalated biliazines linked by a third tetrahedral zinc metal ion. The closure of the ring with zinc ion does not induce the formation of an aromatic ring current in either the pyrazole or indazole-based dimers.

Introduction

For nearly a century, phthalocyanines and their metal adducts have performed key roles as blue or green dyes and pigments.[1–3] Comprised of four isoindoline units linked by sp^2 hybridized nitrogen atoms, phthalocyanine remains important as both a bulk colorant and in increasing roles as an advanced material, useful in applications ranging from light harvesting to catalysis or organic transformations.[4–9] While the chemistry and properties of phthalocyanines and their metal adducts are well understood, much less work has been carried out on the development of phthalocyanine analogue compounds. We have been working on the development of phthalocyanine analogues, which can be defined as isoindoline-based chelate systems that share many of the structural features of normal phthalocyanines.[10–23] Many of these compounds can be produced by using 1,3-diiminoisoindoline (DII) as a precursor.[24,25] DII is commercially available and can be produced in one step from phthalonitrile. DII has shown rich chemistry since it was introduced by Linstead in the early 1950s;[24,25] this compound can be used to form a variety of metal chelating compounds[26–30] as well as a class of phthalocyanine analogues known as the hemiporphyrazines.[31–34]

Several years ago, we introduced the biliazine chelate, a ring-open phthalocyanine analogue comprised of two isoindoline and two pyrazole or indazole units (Scheme 1).[35] For this chemistry, we employed pyrazole or indazole modified DIIs as starting materials, which we have referred to as semihemiporphyrazines.[21] The name biliazine was inspired by the bilin class of heme metabolites, which can bind to metals as an open macrocycle. The biliazine open macrocycle is notable as it forms *via* a template reaction and the ring is closed by a strong hydrogen bond between the pyrazole or indazole subunits. We surmised that this hydrogen bonded pair of heterocycles could potentially coordinate to a metal ion upon deprotonation. Replacing the hydrogen bond with a metal ion would close the ring and potentially affect the electronic structure of the newly formed metallomacrocycle.

In this report, we present the synthesis and characterization of a pair of biliazine dimer complexes. This chemistry represents the first example of such a metal-based ring closure for an isoindoline-based chelate system. While deprotonation and subsequent metal chelation is not a viable route for dimer formation, we were able to use a self-assembly method to afford the metal linked dimers. These compounds have two zinc environments: a square pyramidal zinc ion at the core of the chelates and a second four coordinate Zn(II) site that links the two biliazine units together. We interrogated the spectroscopy and electronic structure using both experimental and theoretical methods, and we deduced that closing of the ring with zinc ion does not induce aromatic ring currents in these systems.

Experimental

General information

All reagents and starting materials were purchased from commercial vendors and used without further purification. The pyrazole and indazole semihemiporphyrazine chelate

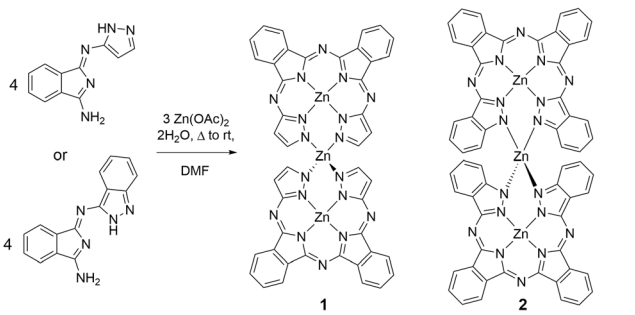

Scheme 1 Synthesis of biliazine dimers **1** and **2**. Axial solvent molecules (DMF and H_2O) on **1** and **2** have been omitted for clarity.

[a]*Department of Chemistry, University of Akron, Akron, OH 44325, USA. E-mail: ziegler@uakron.edu*

[b]*Department of Chemistry, University of Tennessee, Knoxville, TN 37996, USA*

precursors were synthesized according to published procedures.[19,35] Deuterated solvents were purchased from Cambridge Isotope Laboratories and used as received. NMR spectra were recorded on a 300 MHz spectrometer and chemical shifts were given in ppm relative to residual solvent resonances. High-resolution mass spectrometry experiments were performed on a Bruker MicroTOF-III and MicroTOF-qIII instruments. X-ray intensity data were measured on a Bruker CCD-based and PHOTON II CPAD-based diffractometer with dual Cu/Mo ImuS microfocus optics (Cu Kα radiation, $\lambda = 1.54178$ Å, Mo Kα radiation, $\lambda = 0.71073$ Å). Crystals were mounted on a cryoloop using Paratone oil and placed under a steam of nitrogen at 100 K (Oxford Cryosystems). The detector was placed at 5.00 cm from the crystal, and the data were corrected for absorption with the SADABS program. The structures were refined using the Bruker SHELXTL Software Package (Version 6.1)[36] and were solved using direct methods until the final anisotropic full-matrix, least squares refinement of F2 converged. X-ray data collection and structure parameters are presented in Table S1. UV-visible spectra were recorded on a SHIMADZU UV-2600i UV-visible spectrometer.

Synthesis of 1

64 mg (0.303 mmol) of pyrazole semihemiporphyrazine was dissolved in 4 mL of DMF. 50 mg of $Zn(CH_3CO_2)_2 \cdot 2H_2O$ (0.228 mmol) was added to the DMF solution and stirred at room-temperature for 1 hour. After removing the solvent DMF with rotary evaporator, the resultant red powder was washed with MeOH and dried. Yield: 49 mg (64%). ^{1}H NMR (300 MHz, DMSO-d_6): δ (ppm): 8.15 (m, 4H), 7.98 (m, 4H), 7.70 (m, 8H), 7.52 (m, 4H), 6.51 (m, 4H). HRMS (TOF LD+) m/z: calcd for $C_{44}H_{25}N_{18}Zn_3$: 1001.0342, found 1001.0362 ($M + H^+$). Crystals suitable for X-ray diffraction were grown by slow evaporation from DMF, and we observed the formation of two crystal forms (**1a** and **1b**) each with two equivalents of DMF solvate per dimer.

Synthesis of 2

The same procedure was used as for **1** but with 84 mg of indazole semihemiporphyrazine (0.304 mmol) and 50 mg of $Zn(CH_3CO_2)_2 \cdot 2H_2O$ (0.228 mmol). Yield: 54 mg (59%). ^{1}H NMR (300 MHz, py-d_5): δ (ppm): 8.18 (dd, 4H), 7.98 (d, 4H), 7.78 (d, 4H), 7.75 (m, 8H), 7.34 (dd, 4H). 7.21 (t, 4H), 7.11 (t, 4H). HRMS (TOF LD+) m/z: calcd for $C_{60}H_{33}N_{18}Zn_3$: 1201.0974, found 1201.0980 ($M + H^+$). Crystals suitable for X-ray diffraction were grown by slow evaporation from DMF. The crystal included two equivalents of DMF solvate per dimer.

Computational details

The starting geometries of compounds **1** and **2** were optimized using a B3LYP exchange–correlation functional,[37] and were in good agreement with experimentally determined data. Energy minima in optimized geometry were confirmed by the frequency calculations (absence of the imaginary frequencies). The solvent effect was modeled using the polarized continuum model (PCM).[38] In all calculations, DMF was used as the solvent (in the PCM-TDDFT calculation, the first 30 states were calculated. All light atoms were modeled using the 6-311G(d)[39] basis set. Full-electron Wachter's basis set was used for zinc atoms. Gaussian 09 software was used in all calculations.[40] The QM Forge program was used for molecular orbital analysis in all cases.[41]

Results and discussion

Initially, we attempted to insert a metal after synthesis of the biliazine. The zinc biliazine hydrogen bond can be considered as very strong, as it exhibits a chemical shift of 16.73 ppm as well as a N–N distance of ~2.7 Å.[35] Unsurprisingly, the strength of the hydrogen bond is such that moderate bases such as diisopropyl ethylamine (DIPEA), pyridine, or metal acetate salts are unable to deprotonate this position. The significantly stronger organic base 1,8-diazabicycloundec-7-ene (DBU) similarly does not deprotonate zinc biliazine. We can remove the bridging proton by using lithium diisopropylamide, as observed by UV-visible spectroscopy, but strong bases tend to hydrolyse the ring if water is present. Although we are currently optimizing the deprotonation of metal biliazine complexes with lithium salts, we found that a zinc bridged dimer complex could be produced directly *via* self-assembly from pyrazole- or indazole-modified diiminoisoindolines by reacting with an increased number of equivalents of metal acetate salt in DMF solution.

Scheme 1 shows the reaction between the pyrazole and indazole-based DII chelates and an increased number of equivalents of zinc acetate in DMF. Reaction between the chelate precursors and zinc ions in a 4 : 3 ratio results in the formation of biliazine dimers. The resultant compounds were much less soluble than their parent monomeric biliazines, showing only appreciably solubility in DMF and in pyridine. We

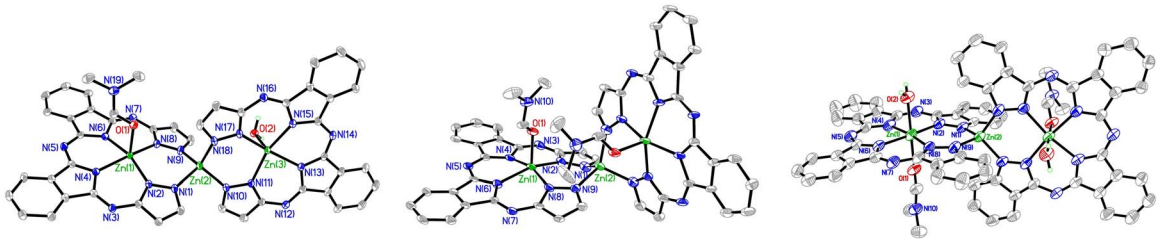

Fig. 1 X-ray crystal structures of **1a** (left), **1b** (middle), and **2** (right) with 50% thermal ellipsoids. Hydrogen atom positions and co-crystallized solvent molecules (two equivalents of DMF per dimer for each structure) have been omitted for clarity.

Table 1 Selected bond lengths (Å) and angles (°) for **1a**, **1b**, and **2**

	1a	**1b**	**2**
Zn–N (macrocycle core) Å	2.0791(19), 2.1192(19), 2.0904(19), 2.0875(19), 2.0869(19), 2.1189(19), 2.1189(19) 2.0859(19)	2.104(5), 2.084(6), 2.115(5), 2.068(5)	2.123(5), 2.100(4). 2.110(5), 2.115(4)
Zn–N (bridging), Å	1.972(2), 1.969(2), 1.950(2), 1.961(2)	1.964(6), 1.964(5)	1.977(4), 1.978(5)
N–Zn–N (bridging), °	108.28(8), 115.02(9), 113.00(9), 106.00(8), 110.59(8), 103.63(8)	120.5(3), 103.6(2), 102.5(2), 125.8(3)	107.4(3), 114.42(18), 106.92(19), 107.0(3)

were able to isolate the dimeric products as pure crystalline solids and we obtained single crystals suitable for X-ray structure determination for both compounds. Two different crystal forms were elucidated for the pyrazole-based biliazine system along with a single crystal form for the indazole variant. The structures of the two forms of **1** and the single form of **2** are shown in Fig. 1. Selected bond lengths and angles for the three structures are shown in Table 1. Both pyrazole-based dimer crystals were grown from DMF, and each exhibits a five coordinate Zn(II) ion at the centre of the chelate with an axial solvent bound through its oxygen atom. In **1a**, the two metal sites have different solvents (water and DMF) while in **1b** the axial solvents are both DMF molecules. In both cases, the two chelate rings are closed and linked together *via* a third Zn(II) ion. The primary difference between the two forms is the relative twist of the two biliazine rings; in one form the two rings are nearly orthogonal, while in the second there is an appreciable bend in the overall structure. The indazole-based dimer **2** exhibits six coordinate zinc centres in each macrocycle unit, with water and DMF each bound on opposite sides of the metal, and the central linking zinc is tetrahedral as observed in **1a** and **1b**. The variation of the equatorial Zn–N bond lengths is greater in **1a** and **1b** (~2.08–2.12 Å) than in **2**, where all such bonds measure between ~2.10 and ~2.12 Å. For the Zn–N bonds at the central metal position, which links the two macrocycles, the lengths are shorter, ranging from an average of ~1.96 in **1a** and **1b** to ~1.98 in **2**. In the latter case, this increase in length is most likely due to the steric bulk of the indazole rings. The orthogonal structures **1a** and **2** exhibit less distortion from tetrahedral, showing angles relatively close to ideal, ranging from ~106° to ~115°. In contrast, **1b** has much greater deviation from ideal angles at the central zinc ion, with angles ranging between ~103° and ~121°.

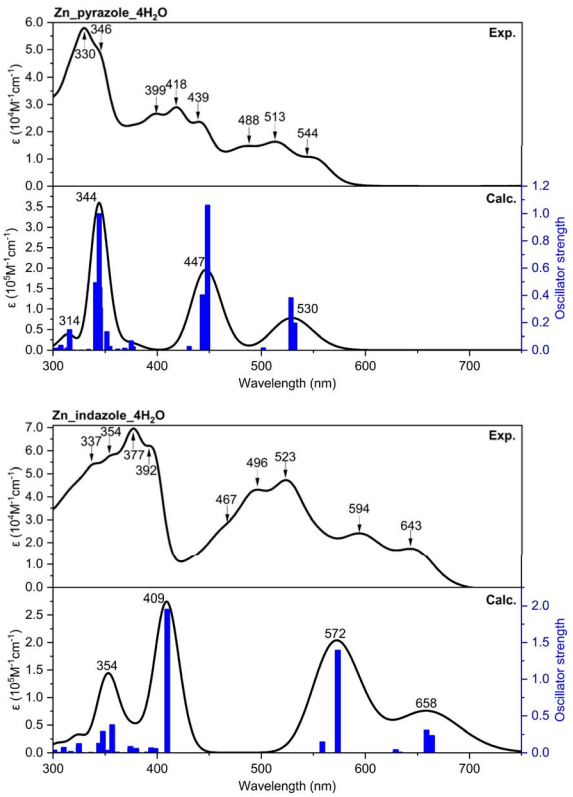

Fig. 2 Experimental and TDDFT calculated spectra for **1** (top) and **2** (bottom) in DMF. Calculations used axial water ligands in place of DMF.

In both **1** and **2**, the central zinc ions effectively close the macrocycle rings through coordination of the pyrazole and indazole units respectively. This ring closure raises the question of the possible induction of aromaticity upon dimer formation. In the biliazine monomer systems, the rings are linked through a hydrogen bond between the pyrazole units, and we did not observe any aromatic cross conjugation in those systems. Based on our observation, the closing of the biliazine ring with zinc ion does not induce any aromatic ring current effects. Experimentally, the lack of aromaticity can be confirmed *via* UV-visible spectroscopy and through NMR spectroscopy. The UV-visible spectrum, shown in Fig. 2, does not exhibit features consistent with an aromatic Gouterman-type four orbital model system.[42–45] The spectra of **1** and **2** resemble that of their parent monomeric systems, and the extinction coefficients, which are on the order of 10^4, are consistent with a non-aromatic conjugated π system. Neither **1** nor **2** exhibit any significant emission upon irradiation. The ^{1}H NMR spectra of **1** and **2**, while missing the distinctive hydrogen bonded proton position in monomeric biliazine, lack significant ring current effects in the observed chemical shifts to attribute any annulene-type aromaticity to either dimer system. Considering the electronic structure of zinc ion, which has highly destabilized p orbitals relative to the π system of the biliazine chelate, it is not surprising that aromaticity is not induced in **1** and **2** upon ring closure and dimerization.

We further probed the electronic structure of **1** and **2** through the use of DFT and TDDFT methods. Fig. 3 shows the frontier orbital energies and structures for compounds **1** and **2**. Orbital composition charts and frontier orbital structures can be seen in the SI file (Fig. S3–S6) Due to their orthogonal structures, the orbitals on each half of the linked dimers

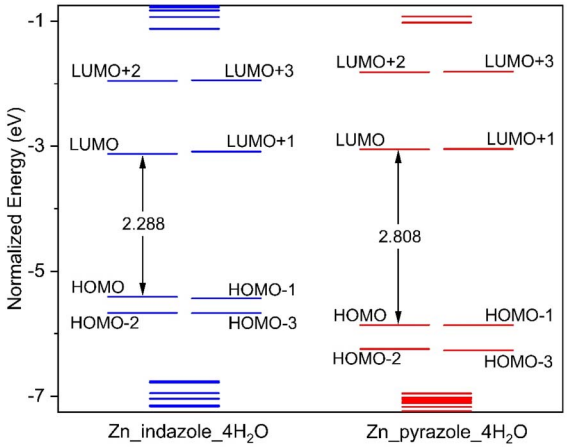

Fig. 3 Simplified frontier energy level diagram of the pyrazole dimer **1** (right) and the indazole dimer **2** (left).

minimally interact. This results in pairs of nearly degenerate orbitals resulting from the contribution of each biliazine unit. Individually, the electronic structure of each portion of the dimer resembles that of monomeric biliazine. The frontier orbital structures for the two compounds exhibit similar distributions of electron density (SI Fig. S5 and S6), and inspection of the atomic orbital composition for the frontier orbitals reveals that these molecular orbitals are primarily π in character (SI Fig. S3 and S4). As observed in monomeric zinc biliazine, the zinc ion orbitals do not play a significant role in the π systems of the dimer. This last aspect of both **1** and **2** helps to explain why the zinc ion bridge does not induce aromatic cross conjugation in either ring system.

In conclusion we have closed the ring in biliazine *via* the synthesis of dimer compounds linked by use of a zinc metal ion. This synthesis occurs through a self-assembly process, and not *via* initial formation and deprotonation of the monomer precursor, as the strongly hydrogen bonded proton position is highly resistant to removal. We were able to construct dimers from both pyrazole and indazole-based isoindoline chelates. The linking zinc ion is tetrahedral, resulting in non-coplanar linked rings. Due to this lack of planarity, there is little electronic interaction between the rings. In addition, due to the closed shell electronic structure of the linking zinc ion, we do not observe the induction of aromaticity in either dimer system. We will continue to explore ring closure and dimer formation in the biliazines and in related modified isoindoline-based systems.

Author contributions

CJZ conceived and directed the research, VNN carried out the computational investigations. TIJ, WYC, BRS, and MTD carried out the experiments. WYC and CJZ elucidated the crystal structures. CJZ, VNN, WYC, and TIJ wrote and edited the manuscript.

Conflicts of interest

There are no conflicts to declare.

Data availability

CCDC 2531175–2531177 contain the supplementary crystallographic data for this paper.[46a–c]

Supplementary information (SI): including experimental procedures, spectroscopy, computational details, and X-ray crystallographic data. See DOI: https://doi.org/10.1039/d6ra01668e.

Acknowledgements

V. N. acknowledges support from NSF (CHE-2153081) C. J. Z. acknowledges support from the University of Akron.

Notes and references

1 P. Gregory, *J. Porphyrins Phthalocyanines*, 2000, **4**, 432–437.
2 P. Erk and H. Hengelsberg, K. M. Kadish, K. M. Smith and R. Guilard, *Porphyrin Handbook*, Elsevier Science, San Diego, CA, 2003, vol. 19, pp. 105–149.
3 G. Zanotti, F. Palmeri and V. Raglione, *Chem. Eur. J.*, 2024, **30**, e202400908.
4 D. Woehrle, G. Schnurpfeil, S. G. Makarov, A. Kazarin and O. N. Suvorova, *Makrogeterotsikly*, 2012, **5**, 191–202.
5 G. de la Torre, P. Vazquez, F. Agullo-Lopez and T. Torres, *J. Mater. Chem.*, 1998, **8**, 1671–1683.
6 A. B. Sorokin, *Chem. Rev.*, 2013, **113**, 8152–8191.
7 A. M. Schmidt and M. J. F. Calvete, *Molecules*, 2021, **26**, 2823.
8 Z. Li, Z. Zhou, M. Sun, T. Wu, Q. Lu, L. Lu, B. Chen, C. H. Chan, H. H. Wonga and B. Huang, *Chem. Sci.*, 2025, **16**, 14019–14037.
9 P.-C. Lo, M. S. Rodríguez-Morgade, R. K. Pandey, D. K. P. Ng, T. Torres and F. Dumoulin, *Chem. Soc. Rev.*, 2020, **49**, 1041–1056.
10 I.-S. Tamgho, A. Hasheminasab, J. T. Engle, V. N. Nemykin and C. J. Ziegler, *J. Am. Chem. Soc.*, 2014, **136**, 5623–5626.
11 I.-S. Tamgho, J. T. Engle and C. J. Ziegler, *J. Org. Chem.*, 2012, **77**, 11372–11376.
12 L. A. Crandall, H. M. Rhoda, V. N. Nemykin and C. J. Ziegler, *New J. Chem.*, 2016, **40**, 5675–5678.
13 A. J. Osinski, T. Blesener, A. Hasheminasab, C. Holstrom, V. N. Nemykin, R. S. Herrick and C. J. Ziegler, *Inorg. Chem.*, 2016, **55**, 12527–12530.
14 I.-S. Tamgho, L. A. Crandall, J. T. Engle and C. J. Ziegler, *Inorg. Chem. Commun.*, 2017, **76**, 122–124.
15 B. R. Schargae, K. Chanawanno, L. A. Crandall and C. J. Ziegler, *J. Porphyrins Phthalocyanines*, 2020, **24**, 129–134.
16 B. R. Schrage, D. Vitale, K. A. Kelly, V. N. Nemykin, R. S. Herrick and C. J. Ziegler, *J. Organomet. Chem.*, 2020, **919**, 121331.
17 S. Gaire, B. R. Schrage, V. N. Nemykin and C. J. Ziegler, *Dalton Trans.*, 2021, **50**, 826–829.
18 B. R. Schrage, V. N. Nemykin and C. J. Ziegler, *Org. Lett.*, 2021, **23**, 1076–1080.
19 B. R. Schrage, V. N. Nemykin and C. J. Ziegler, *Org. Lett.*, 2021, **23**, 5246–5250.

20 B. R. Schrage, C. A. Farmer, V. N. Nemykin and C. J. Ziegler, *J. Porphyrins Phthalocyanines*, 2021, **25**, 1048–1054.
21 S. Gaire, B. R. Schrage, V. N. Nemykin and C. J. Ziegler, *Eur. J. Inorg. Chem.*, 2022, **2022**, e202200155.
22 J. Bore, W.-Y. Chen, V. N. Nemykin and C. J. Ziegler, *J. Porphyrins Phthalocyanines*, 2024, **28**, 429–434.
23 B. R. Schrage, S. Gaire, K. Mamattah, D. E. Nevonen, V. N. Nemykin and C. J. Ziegler, *Inorg. Chem. Front.*, 2024, **11**, 3937–3940.
24 J. A. Elvidge and R. P. Linstead, *J. Chem. Soc.*, 1952, 5000–5007.
25 P. F. Clark, J. A. Elvidge and R. P. Linstead, *J. Chem.Soc.*, 1953, 3593–3601.
26 G. Reshma, V. Padmanabhan, A. R. Varma, M. S. Gouri, U. R. Nair, P. B Parvathy, N. V. Kulkarni and D. Senthurpandi, *J. Mol. Struct.*, 2021, **1226**, 129344.
27 B. Siggelkow, M. B. Meder, C. H. Galka and L. H. Gade, *Eur. J. Inorg. Chem.*, 2004, **17**, 3424–3435.
28 E. W. Wong, J. S. Ovens and D. B. Leznoff DB, *Chem. Eur. J.*, 2012, **18**, 6781–6787.
29 J. O. Wenzel, I. Fernández and F. Breher, *Eur. J. Inorg. Chem.*, 2023, **2624**, e202300315.
30 P. Zhang, H. Liao, H. Wang, X. Li, F. Yang and S. Zhang, *Organometallics*, 2017, **36**, 2446–2451.
31 F. Fernández-Lázaro, T. Torres, B. Hauschel and M. Hanack, *Chem. Rev.*, 1998, **2**, 563–576.
32 A. Muranaka, S. Ohira, D. Hashizume, H. Koshino, F. Kyotani, M. Hirayama and M. Uchiyama M, *J. Am. Chem. Soc.*, 2012, **1**, 190–193.
33 V. Persico, M. Carotenuto and A. Peluso, *J. Phys. Chem. A*, 2004, **18**, 3926–3931.
34 Y. Tanaka, T. Murayama, A. Muranaka, E. Imai and M. Uchiyama, *Chem. Eur. J.*, 2020, **8**, 1768–1771.
35 B. R. Schrage, V. N. Nemykin and C. J. Ziegler, *Chem. Commun.*, 2020, **56**, 6628–6631.
36 G. M. Sheldrick, *Acta Crystallogr. Sect. A Found. Crystallogr.*, 2008, **64**, 112–122.
37 J. Tao, J. P. Perdew, V. N. Staroverov and G. E. Scuseria, *Phys. Rev. Lett.*, 2003, **91**, 1–4.
38 J. Tomasi, B. Mennucci and R. Cammi, *Chem. Rev.*, 2005, **105**, 2999–3093.
39 A. D. McLean and G. S. Chandler, *J. Chem. Phys.*, 1980, **72**, 5639–5648.
40 M. J. Frisch, G. W. Trucks, H. B. Schlegel, G. E. Scuseria, Ma. Robb, J. R. Cheeseman, G. Scalmani, V. Barone, B. Mennucci, and G. A. Petersson, *et al.*, *Gaussian 09, Revision D.01*, Gaussian Inc., Wallingford, CT.
41 A. L. Tenderholt, *QMForge: A Program to Analyze Quantum Chemistry Calculations*, Version 3.0, https://qmforge.net.
42 M. J. Gouterman, in *The Porphyrins*, ed. Dolphin, D., Academic Press: New York, 1978, vol. 3, pp. 1–165.
43 M. J. Gouterman, *Mol. Spectrosc.*, 1961, **6**, 138–163.
44 M. J. Gouterman, G. Wagniere, L. C. Snyder and L. C. J, . *Mol. Spectr.*, 1963, **11**, 108–127.
45 C. Weiss, H. Kobayashi and M. J. Gouterman, *J. Mol. Spectr.*, 1965, **16**, 415–450.
46 (*a*) CCDC 2531175: Experimental Crystal Structure Determination, 2026, DOI: 10.5517/ccdc.csd.cc2qywtd; (*b*) CCDC 2531176: Experimental Crystal Structure Determination, 2026, DOI: 10.5517/ccdc.csd.cc2qywvf; (*c*) CCDC 2531177: Experimental Crystal Structure Determination, 2026, DOI: 10.5517/ccdc.csd.cc2qywwg.